Analysis of the Flux Consumption and Metal Transfer for Tandem Submerged Arc Welding Process under Iso-Heat Input Conditions

A study was performed on flux consumption for tandem SAW

BY D.-W. CHO, D. V. KIRAN, AND S.-J. NA

ABSTRACT

The tandem submerged arc welding process brings higher productivity and better mechanical properties for the materials involved. In this study, constant heat input per unit length (2.5 kJ/mm) was maintained and flux consumption per unit length was analyzed for different welding conditions. The physical analysis, including arc interaction and metal transfer mode along the current value, were considered for understanding flux consumption. The relationship among flux consumption per unit length, metal transfer mode, and resultant weld bead shapes was analyzed. Especially, it was found out that flux-wall guided transfer plays an important role in forming the fusion zone in the low-current tandem submerged arc welding processes.

KEYWORDS

• Submerged Arc Welding (SAW) • Tandem Welding • Flux Consumption
• Flux-Wall Guided Transfer • Iso-Heat Input

Introduction

The two-wire tandem submerged arc welding (SAW-T) process is a high-deposition variant of the conventional single-wire submerged arc welding process (SAW). Nowadays, the heavy fabrication industries are replacing double-sided SAW of medium to thick plates with single-sided, single-pass tandem SAW (Refs. 1, 2). The flux consumption rate in the SAW process has a significant influence on the final weld mechanical properties (Ref. 3). Understanding the influence of different process parameters on the flux consumption rate is important to control the final weld quality. However, the presence of numerous process parameters associated with the multiple arcs in the SAW-T process increases the complexity of the process and makes it more difficult to understand their influence on the flux consumption rate. Furthermore, for a constant heat input, the variation in the leading and trailing arcs' current can have a complex influence on the flux consumption rate. Hence, a detailed analysis of process parameters is critical for a better understanding of the weld quality variation in relation to the process parameters.

Although significant efforts have been made to understand flux consumption in the SAW process, there has been little corresponding research on the SAW-T process. Renwick and Patchett (Ref. 4) observed the effect of welding current and wire diameter on flux consumption in the SAW process. They reported that for a given wire diameter, flux consumption increased with an increase in the welding current to a certain level called the transition current. A further increase in the welding current above the transition level decreased flux consumption. On the other hand, the transition current decreased with an increase in wire diameter. Chandel (Ref. 5) performed a detailed study on the influence of welding current polarity, voltage, and electrode extension on the flux consumption rate in the SAW process. An increase in arc voltage and electrode extension improved the flux consumption rate. Compared to direct current electrode negative polarity, a low flux consumption rate was reported at direct current electrode positive polarity. Tusek et al. (Ref. 6) compared the flux consumption rate in the single, two-wire tandem, and three-wire tandem submerged arc welding processes. They reported that, for a constant current, the flux consumption rate decreased with an increase in the number of wires. Chai (Ref. 7) suggested that in the high-temperature environment near the welding plasma, all oxides in the flux were susceptible to decomposition and produced oxygen.

D.-W. CHO is with Thermal Hydraulics Safety Research Division, KAERI, Daejeon, Republic of Korea. D. V. KIRAN and S.-J. NA (sjna@kaist.ac.kr) *are with Department of Mechanical Engineering, KAIST, Daejeon, Republic of Korea.*

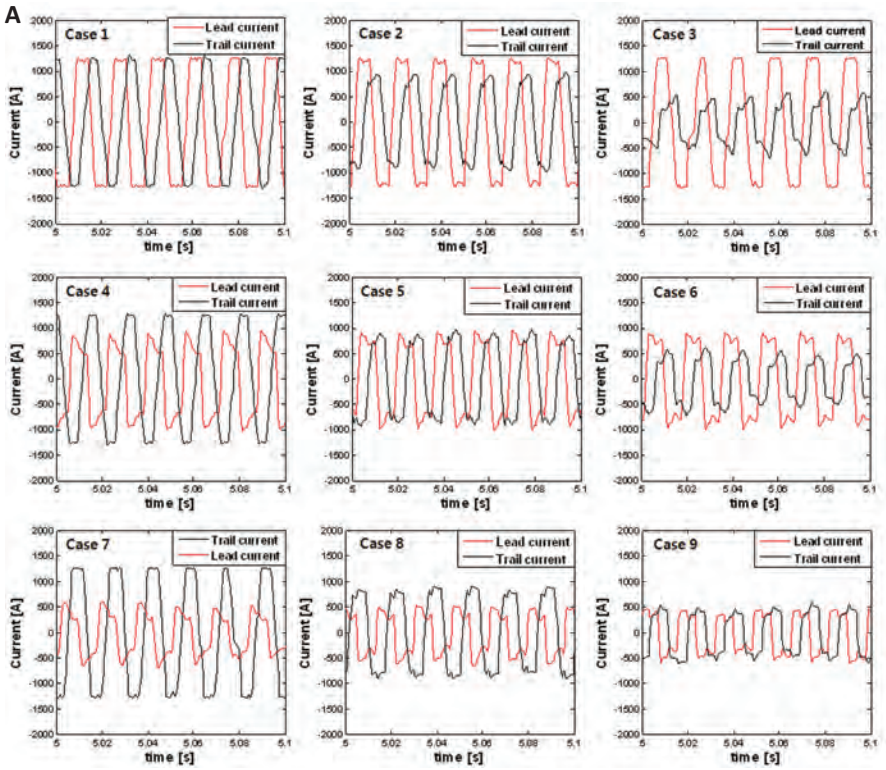

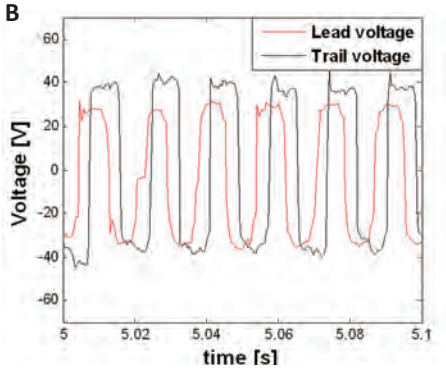

Fig. 1 — Welding signals in the experiment: A — Current; B — voltage.

Table 1 — Welding Conditions (Ref. 14)

Group	Case	Current of leading electrode (A, RMS)	Voltage of leading electrode (V, RMS)	Current of trailing electrode (A, RMS)	Voltage of trailing electrode (V, RMS)	Welding speed (mm/s)	Heat input per unit length (kJ/mm)
A	1	1000	32	1000	35	26.81	2.5
	2	1000	32	700	35	22.60	2.5
	3	1000	32	400	35	18.41	2.5
B	4	700	32	1000	35	22.96	2.5
	5	700	32	700	35	18.76	2.5
	6	700	32	400	35	14.56	2.5
C	7	400	32	1000	35	19.12	2.5
	8	400	32	700	35	14.92	2.5
	9	400	32	400	35	10.72	2.5

Based on the subsequent reaction with the weld pool, oxide inclusions were generated. The modified basicity index formula proposed by Eagar et al. (Ref. 8) correlates well with the oxygen content in SA welds. These oxide inclusions in steel welds can affect the formation of acicular ferrite, which improves the weld metal toughness (Ref. 9). However, excessive weld metal oxygen and the subsequent oxide inclusions can deteriorate weld metal mechanical properties. Kanjilal et al. (Ref. 10) studied the combined effect of flux and welding parameters on the chemical composition and mechanical properties of SA weld metal. Sharma et al. (Ref. 11) studied the effect of the magnetic field generated in the vicinity of the two arcs on the flux consumption rate in twin-wire SAW. They reported the magnetic field became concentrated with dissimilar wire diameters, which in turn narrowed the arc deflection. This eventually resulted in lower flux consumption. Cho et al. (Ref. 12) made a slag heat input model from the flux consumption rate for single-electrode SAW using computational fluid dynamics (CFD). They found the slag heat input from the molten slag in high-current SAW is much smaller than that from the arc plasma. Kiran et al. (Ref. 13) made an attempt to understand the arc behavior in the two-wire and three-wire tandem submerged arc welding process. The arc interaction models were developed to estimate the arc's deflection. Furthermore, the molten pool behavior in the tandem processes and its subsequent influence on the weld bead microstructure were studied for different leading and trailing arc currents at a constant heat input of 2.5 kJ/mm. However, no information on the influence of the process parameters and the arc deflection on the flux consumption has been reported (Refs. 14–16).

In summary, to date no work has been reported on how to understand the influence of the leading and trailing arcs' current on flux consumption at a constant heat input. As evident from the previous studies, it is very important to understand the flux consumption rate in the SAW-T process in detail to attain desirable microstructure and subsequent mechanical properties. An experimental investigation on the flux consumption rate is presented in this study for a wide range of leading and trailing arcs' current at a constant heat input of 2.5 kJ/mm. The measured variation in the flux consumption rate is then explained with respect to the weld bead profiles and the arc interaction.

Experimental Setup

The AC signals have more advantages than DC signals in the welding process. Because it is possible to control the detail variations such as EN ratio and phase shift, it is easy to control the welding process specifically. This study used the same experiment conditions as in previous studies that adopted AC welding signals (current and voltage) (Refs. 12, 14). For both leading and

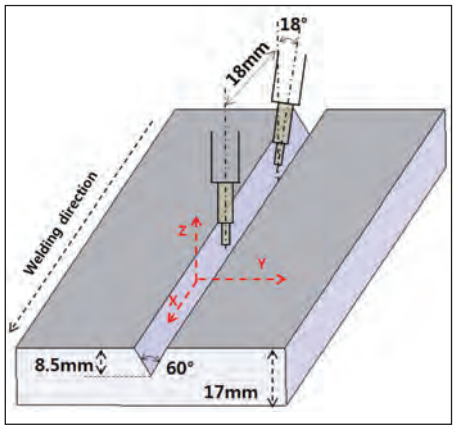

Fig. 2 — Schematic sketch of experimental setup (Ref. 14).

trailing electrodes, this study adopted tandem AC polarity with 60-Hz trapezoidal wave as shown in Fig. 1A, B. Figure 2 presents a schematic sketch of the V-groove materials and the electrode positions. The distance between the electrodes is 18 mm and the phase shift is 90 deg, respectively. The heat input per unit lengths (2.5 kJ/mm) were kept constant while the combination of the current (3 × 3) and the corresponding welding speed along the different welding conditions were varied as written in Table 1. This study used solidified slag (Fig. 3) because it was assumed to be a consumed flux during the SAW process. The solidified slag weight and length are given in Table 2.

Results and Discussion

Analysis of Flux Consumption

The weight of consumed flux can be assumed to be the same as the weight of solidified slag in the SAW process. This study measured the weight and length of the solidified slag, and then extracted slag weight per length (SWPL) as shown in Table 2. It is meaningful to compare SWPL values along the different welding conditions (cases 1 to 9) within the same heat input (2.5 kJ/mm). Cases 1 to 9 demonstrate that the bead width is linearly proportional to the SWPL (R^2 = 0.8917), as shown in Fig. 4, because if the bead width increases inside the flux cavity, the contact region between molten pool and slag as shown in Fig. 5 should increase. Additionally, the bead widths for all nine

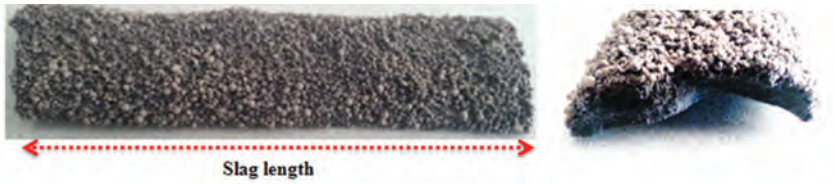

Fig. 3 — Solidified SAW slag.

Table 2 — Slag Weight, Length, and Bead Width

Group	Case	Slag weight (g)	Slag length (mm)	Bead width (mm)	Slag weight per length (g/mm)
A	1	30.1	250	12.03	0.120
	2	49.0	265	12.51	0.185
	3	51.6	295	12.29	0.175
B	4	46.0	195	14.20	0.236
	5	56.7	250	14.46	0.227
	6	55.5	245	15.05	0.227
C	7	58.0	250	15.27	0.232
	8	72.8	270	15.96	0.270
	9	95.4	295	17.00	0.323

cases along the weld interface are normally stable.

The increase in bead width is closely related to the molten pool behavior in SAW-T where the arc interaction and metal transfer heavily impact on the molten pool behavior and corresponding fusion zone (Ref. 14). Considering the pinch effect on the arc plasma in the tandem arc welding process, it was found that the arc plasmas of the leading and the trailing electrodes attracted each other when the current polarities of two electrodes were the same; however, the arc plasmas of two electrodes repulsed each other when the current polarities were different. Kiran et al. (Ref. 13) observed the arc displacement in the tandem arc welding process and made the arc displacement models as shown in Equations 1 and 2.

$$X_L = C_1\left(\frac{I_T}{I_L}\right)\left(\frac{l_L^2}{d}\right) \qquad (1)$$

$$X_T = C_2\left(\frac{I_L}{I_T}\right)\left(\frac{l_L^2}{d}\right) \qquad (2)$$

where X_L and X_T are the arc center displacement for leading and trailing electrodes. Thus, it can be expected that a higher current arc plasma can be more stable than a lower current arc plasma, while a lower current arc plasma can be shifted more due to the arc interaction effect.

Previous research (Refs. 4, 5) reported the flux consumption increased until the transient current value, and the flux consumption started to decrease when the welding current was higher than transient current. Cho et al. (Ref. 12) were concerned about this flux consumption pattern and they assumed spray metal transfer could be performed in high-current, single-electrode SAW. Moreover, they applied the spray metal transfer mode in CFD simulation and the model was validated by comparing the experiment results. Kiran et al. (Ref. 13) also observed the droplet free-flight direction in high-current (I ≥ 700 A) tandem arc welding and found that the droplet flew to the arc plasma center when it was just detached. So the droplet free-flight depends on the arc interaction effect for high-current welding models. Cho et al. (Ref. 14) adopted this spray transfer droplet flight model as shown in Fig. 6 and the arc interaction models for high-current SAW-T process to calculate the molten pool flow with CFD simulations. As the simulation results showed good agreement with the experiment ones, it is possible to assume the metal transfer mode inside the flux cavity for high-current (I ≥ 700 A) SAW-T is the spray transfer mode. On the other hand, it might not be possible to assume spray

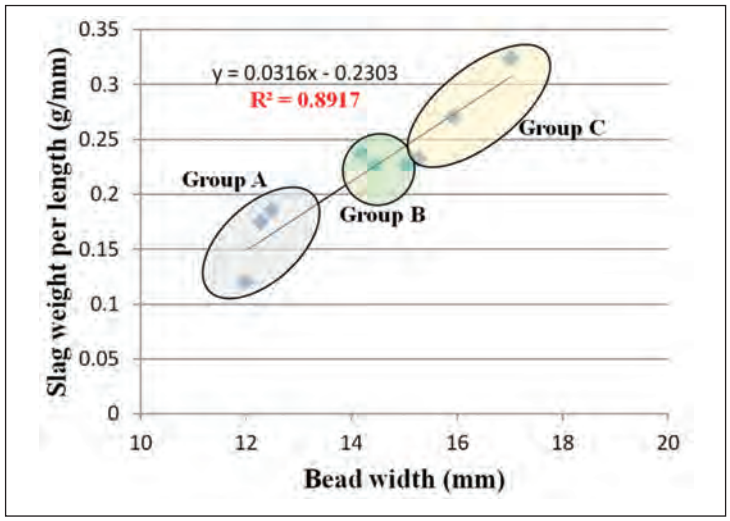

Fig. 4 — The relation between bead width and SWPL.

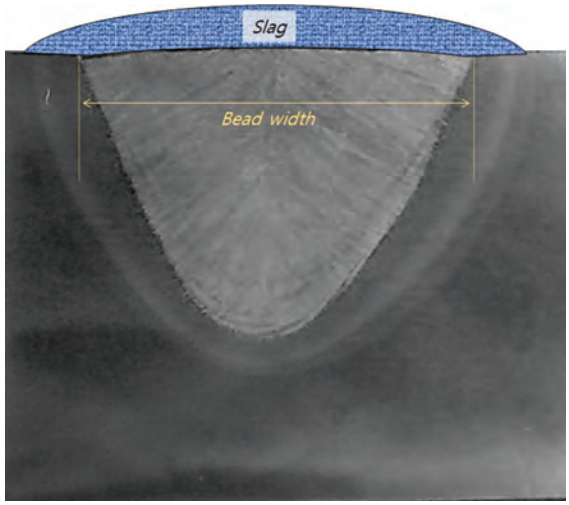

Fig. 5 — Schematic of solidified slag on bead width in tandem SAW.

Table 3 — Difference of SWPL along the Current Combinations

Current Combination	SWPL			
	P (Current of LE > Current of TE)		Q (Current of LE < Current of TE)	
1000 A, 700 A	L1000, T700 (Case 2)	0.185	L700, T1000 (Case 4)	0.236
1000 A, 400 A	L1000, T400 (Case 3)	0.175	L400, T1000 (Case 7)	0.232
700 A, 400 A	L700,T400 (Case 6)	0.227	L400, T700 (Case 8)	0.270

transfer in the low-current model even though there was arc interaction because the electromagnetic force of the electrodes is not enough to form the molten droplet in the case where the wire diameter is big (wire diameter >3.2). Therefore, spray transfer metal transfer is not expected for low-current SAW and this research proposed flux-wall guided transfer in SAW.

Figure 7 shows the schematic of flux and flux wall that is made of molten slag in SAW-T. As the leading electrode (LE) is ahead of the trailing electrode (TE) along the welding direction, the energy heat sources (arc plasma and molten droplet) from the LE can be transferred to the flux near the LE and then form the flux wall (Part I) where the amount of heat transfer from the TE is relatively small. Thus, it can be considered that the solid flux initially melts around Part I. The molten slag generated in this region, therefore, can be expected to take a big portion of total flux consumption.

On the other hand, the amount of energy heat source needed to form the flux wall (molten slag) near TE (Part II) is somewhat different from that in Part I. Some portion of molten slag in Part II seems to be already melted near the LE because two electrodes can move fast at a high welding speed, while the entire molten slag cannot move as fast as the electrodes and the direction of molten slag movement is locally different. Therefore, there is a relative velocity difference between the electrodes and molten slag so that the same molten slag in Part I can move to Part II during SAW-T. Although the energy heat sources (arc plasma and molten droplet) from the TE affect Part II, the amount of molten slag generated in Part II is smaller than that in Part I because some of the energy heat sources from the TE can be transferred to the molten slag instead of the solid flux.

This mechanism can explain the different amounts of SWPL for opposite current combinations as listed in Table 3. When the current of the TE is larger than that of the LE (Q column), SWPL is larger than that of the opposite cases (P column) because X_L values in the Q column are larger than those in the P column. In other words, the higher welding current of the trailing electrode can produce a larger value of X_L, so that the amount of droplet and arc heat flux from the LE can contact the flux wall more in Part I. Finally, more molten slag is produced in Q column conditions.

On the other hand, a smaller amount of molten slag is formed in P column conditions. Even though the droplet and arc heat flux from the LE contact the flux wall in Part I, the X_L values are smaller than in the Q column conditions; therefore, a smaller amount of molten slag is generated.

Analysis of Fusion Zone Shape

The current of the LE from group A in Table 1 is 1000 A. In case 1, the current of the TE is 1000 A, so X_L and the droplet impingement (DI) range of the LE shifts most widely in group A. Therefore, the arc forces and DI from the LE is less focused in the weld pool, as shown in Fig. 7. The resultant penetration is smaller than in other cases in group A, as shown in Fig. 8.

Cho et al. (Ref. 14) found the bead width increases when the arc plasma of the TE approaches the weld pool surface. The variation of X_T and the DI range of the TE in case 2 are wider

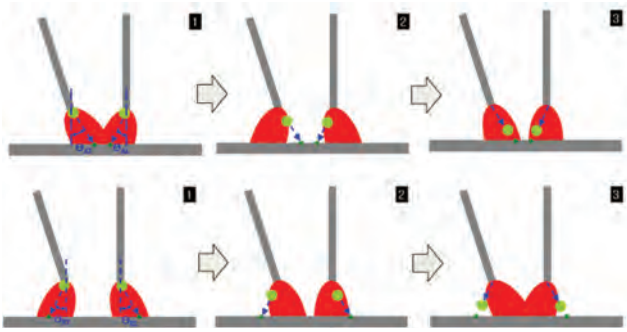

Fig. 6 — Droplet flights due to the arc interaction effects in SAW-T (Ref. 14).

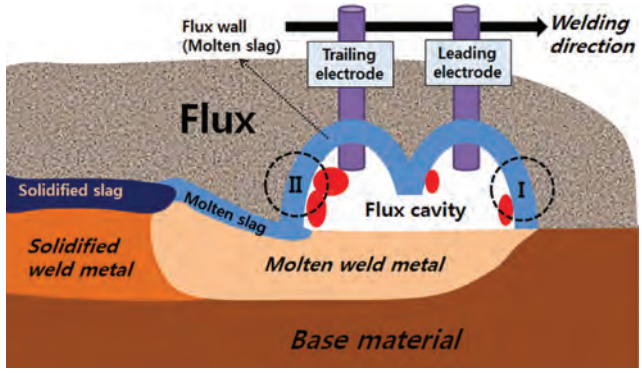

Fig. 7 — Schematic diagram of tandem SAW.

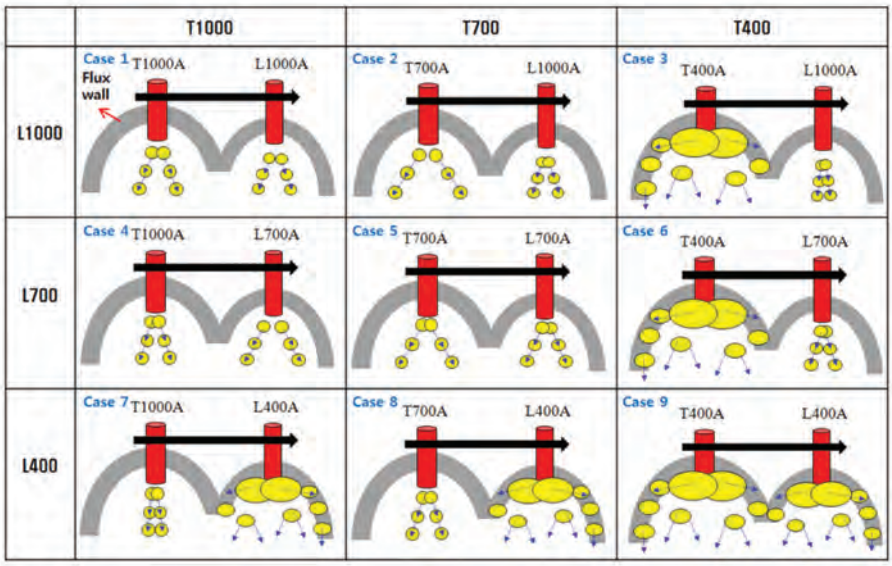

Fig. 8 — Expected metal transfer mode in SAW-T.

than that in case 1; therefore, the bead width in case 2 is larger than that in case 1 (as shown in Figs. 8 and 9). Consequently, the bead width in case 1 is narrower than other cases in group A due to a small variation of X_T and the DI range (Ref. 14).

However, the mechanism of the bead width expansion in case 3 is very different from that in cases 1 and 2. As the current of the TE in case 3 is 400 A, it can be explained by the flux-wall guided (FWG) transfer where the droplets collide with the flux wall and then slide down to the weld pool, as shown in Fig. 8. The molten slag is combined with collided droplets so that the heat input from the molten slag, which is the outer boundary of the arc plasma, is transferred to the upper boundary of the material surface. Additionally, the penetration in case 3 is deeper than in other cases because the variation of X_L is smaller than in other cases, and the arc stiffness of the LE is the strongest among all the cases.

The current of the LE of group B in Table 1 is 700 A. In cases 4 and 5, it is clear that the DI range of the LE is relatively wider than that in cases 1 and 2 (Ref. 14). Therefore, the penetrations of cases 4 and 5 are shorter than those of cases 1 and 2; moreover, a bowl-shaped fusion zone is formed.

On the other hand, the fusion zone shape in case 6 is different from cases 4 and 5. The metal transfer of the LE and the TE is expected in the spray and the FWG modes, respectively. The low current of the TE induces a narrow variation of X_L so that the arc forces and DI of the LE are focused on the weld pool, as shown in Fig. 8. Thus, penetration increases under the LE and the bead width increases due to the FWG transfer from the TE. Finally, the fingertip-shaped fusion zone is formed in case 6. However, the resultant penetrations, bead widths, and corresponding SWPL in case 6 are very similar to those in cases 4 and 5, as shown in Fig. 9.

The current of the LE of group C in Table 1 is 400 A; therefore, the metal transfer mode of the LE in group C is FWG transfer, which produces a relatively shallow penetration. In case 7, the molten metal from the LE by FWG transfer fills in the V-groove, and then the penetration increases when the arc plasma and DI from the TE approaches. Among group C, the penetration of case 7 is deeper than the other cases because the current of the TE is high (1000 A), so it can be explained by the strong arc forces and spray mode metal transfer from the TE. That means that, although the molten pool from the LE already fills in the V-groove by FWG transfer and there is a "cushion effect" when the droplet from the TE impacts the weld pool, the strong arc forces and spray mode metal transfer from the TE can increase the penetration in case 7. Similar to case 7, there is an increase of penetration by the TE (arc forces and spray mode metal transfer) in case 8; on the other hand, the bead width in case 8 is wider than that in case 7 because the variation of X_L and the DI range in case 8 are relatively wider.

In case 9, the metal transfer from both the LE and TE are FWG transfer, and incomplete penetration is induced, as shown in Fig. 9. The molten droplets from both electrodes contact the flux wall, and then it slides down to the upper material surface and fills in the V-groove; however, it is expected that the momentum from the arc forces (arc pressure, electromagnetic force) and the DI do not increase penetration. Even though the capillary force seems to extract the molten pool

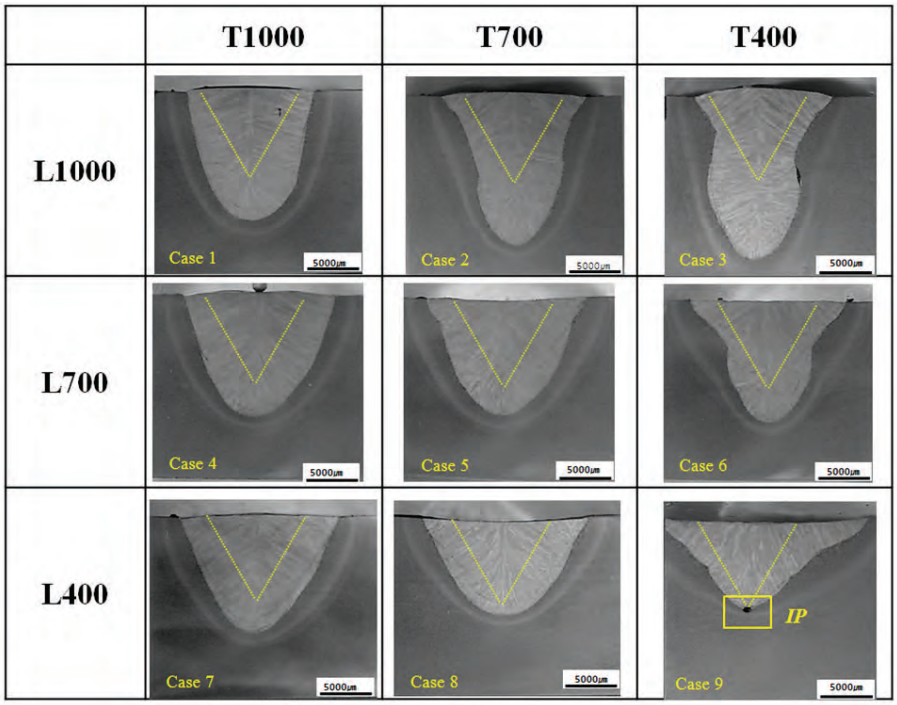

Fig. 9 — Macrosection for nine cases (L: leading, T: trailing).

to fill in the V-groove joint, the void region cannot be filled with the molten fluid and porosity is formed. As the metal transfer from both the LE and the TE is expected FWG transfer, the bead width increases significantly; therefore, the SWPL in case 9 is higher than in the other eight cases.

Conclusions

Flux consumption and metal transfer were analyzed for the SAW-T process. The results of this study are summarized as follows:

1) Although the same heat input (2.5 kJ/mm) was applied in the SAW-T process, the SWPL and bead shapes are different in all nine cases investigated in this study. Moreover, it was found that SWPL is linearly proportional to the weld bead width.

2) SWPL values increase when the current of the TE is higher than that of the LE. This is closely related to the arc interaction effect in the SAW-T process

3) If the current of the TE decreases for a high current (I = 1000 A) LE, the penetration increases. However, if the current of the TE decreases for a low current (I = 400 A) LE, the penetration decreases and the bead width increases. Thus, it can be concluded that the arc interaction effect and metal transfer mode induce a considerable effect on the weld bead shapes.

4) FWG metal transfer produces a wide bead width, but does not result in deep penetration. When the current of both electrodes is low (I = 400 A), it is possible to observe porosity due to incomplete penetration.

Acknowledgments

The authors gratefully acknowledge the support of the Brain Korea 21 plus project, the National Research Foundation of Korea (NRF) grant funded by the Korea government (MSIP). (No. 2012M2A8A2025638) and Mid-career 363 Researcher Program through NRF (2013-015605).

References

1. Kiran, D. V., Basu, B., and De, A. 2012. Influence of process variables on weld bead quality in two wire tandem submerged welding of HSLA steel. *Journal of Materials Processing Technology* 212(10): 2041–2050.

2. Kiran, D. V., Alam, S. A., and De, A. 2013. Development of process maps in two wire tandem submerged arc welding process of HSLA steel. *Journal of Materials Engineering and Performance* 22(4): 988–994.

3. Kou, S. 2002. *Welding Metallurgy*, 2nd edition. New Jersey: Wiley.

4. Renwick, B. G., and Patchett, B. M. 1976. Operating characteristics of the submerged arc process. *Welding Journal* 55(3): 69-s to 76-s.

5. Chandel, R. S. 1998. The effect of process parameters on the flux consumption in submerged arc welding. *Materials and Manufacturing Processes* 13(2): 181-188.

6. Tusek, J., Umek, I., and Bajcer, B. 2005. Weld-cost saving accomplished by replacing single wire submerged arc welding with triple wire welding. *Science and Technology of Welding and Joining* 10(1): 15–22.

7. Chai, C. S., and Eagar, T. W. 1982. Slag metal reactions in binary CaF_2-metal oxide welding fluxes. *Welding Journal* 16(7): 229-s to 232-s.

8. Eagar, T. W. 1978. Sources of weld metal oxygen contamination during submerged arc welding. *Welding Journal* 57(3): 76-s to 80-s.

9. Grong, O., and Matlock, D. K. 1986. Microstructural development in mild and low alloy steel weld metals. *International Metals Reviews* 31(1): 27–48.

10. Kanjilal, P., Pal, T. K., and Majumdar, S. K. 2006. Combined effect of flux and welding parameters on chemical composition and mechanical properties of submerged arc weld metal. *Journal of Materials Processing Technology* 171(2): 223–231.

11. Sharma, A., Arora, N., and Mishra, B. K. 2008. Mathematical modeling of flux consumption during twin wire welding. *International Journal of Advanced Manufacturing Technology* 38(11): 1114–1124.

12. Cho, D. W., Song, W. H., Cho, M. H., and Na, S. J. 2013. Analysis of submerged arc welding process by three-dimensional computational fluid dynamics simulations. *Journal of Materials Processing Technology* 213(12): 2278–2291.

13. Kiran, D. V., Cho, D. W., Song, W. H., and Na, S. J. 2014. Arc behaviour in two wire tandem submerged arc welding. *Journal of Materials Processing Technology* 214(8): 1546–1556.

14. Cho, D. W., Kiran, D. V., Song, W. H., and Na, S. J. 2014. Molten pool behaviour in the tandem submerged arc welding process. *Journal of Materials Processing Technology* 214(11): 2233–2247.

15. Kiran, D. V., Cho, D. W., Lee, H. K., Kang, C. Y., and Na, S. J. 2015. A study on the quality of two wire tandem submerged arc welds under iso-heat input conditions. *The International Journal of Advanced Manufacturing Technology* 78(1–4): 53–62.

16. Kiran, D. V., Cho, D. W., Song, W. H., and Na, S. J. 2015. Arc interaction and molten pool behavior in the three wire submerged arc welding process. *International Journal of Heat and Mass Transfer* 87: 327–340.